RESEARCH ARTICLE

SmartMat WILEY
Open Access

Thermally activated delayed fluorescence materials for nondoped organic light-emitting diodes with nearly 100% exciton harvest

Xiao-Chun Fan[1] | Kai Wang[1] | Yi-Zhong Shi[2] | Dian-Ming Sun[1,3] | Jia-Xiong Chen[1,4] | Feng Huang[1] | Hui Wang[1] | Jia Yu[1] | Chun-Sing Lee[4] | Xiao-Hong Zhang[1]

[1]Institute of Functional Nano & Soft Materials (FUNSOM), Jiangsu Key Laboratory for Carbon-Based Functional Materials & Devices, Joint International Research Laboratory of Carbon-Based Functional Materials and Devices, Soochow University, Suzhou, China

[2]Research Center for Green Printing Nanophotonic Materials, Jiangsu Key Laboratory for Environmental Functional Materials, School of Materials Science and Engineering, Suzhou, China

[3]Organic Semiconductor Centre, EaStCHEM School of Chemistry, University of St Andrews, St Andrews, UK

[4]Center of Super-Diamond and Advanced Films (COSDAF) and Department of Chemistry, City University of Hong Kong, Hong Kong, China

Correspondence

Kai Wang and Xiao-Hong Zhang, Institute of Functional Nano & Soft Materials (FUNSOM), Jiangsu Key Laboratory for Carbon-Based Functional Materials & Devices, Joint International Research Laboratory of Carbon-Based Functional Materials and Devices, Soochow University, 199 Ren'ai Rd, 215123 Suzhou, China.
Email: wkai@suda.edu.cn and xiaohong_zhang@suda.edu.cn

Chun-Sing Lee, Center of Super-Diamond and Advanced Films (COSDAF) and Department of Chemistry, City University of Hong Kong, Hong Kong, China.
Email: apcslee@cityu.edu.hk

Abstract

High-performance nondoped organic light-emitting diodes (OLEDs) are promising technologies for future commercial applications. Herein, we synthesized two new thermally activated delayed fluorescence (TADF) emitters that enable us, for the first time, to combine three effective approaches for enhancing the efficiency of nondoped OLEDs. First, the two emitters are designed to have high steric hindrances such that their emitting cores will be suitably isolated from those of their neighbors to minimize concentration quenching. On the other hand, each of the two emitters has two stable conformations in solid films. In their neat films, molecules with the minority conformation behave effectively as dopants in the matrix composing of the majority conformation. One hundred percent exciton harvesting is thus theoretically feasible in this unique architecture of "self-doped" neat films. Furthermore, both emitters have relatively high aspect ratios in terms of their molecular shapes. This leads to films with preferred molecular orientations enabling high populations of horizontal dipoles beneficial for optical out-coupling. With these three factors, OLEDs with nondoped emitting layers of the respective emitters both achieve nearly 100% exciton utilization and deliver over 30% external quantum efficiencies and ultralow efficiency roll-off at high brightness, which have not been observed in reported nondoped OLEDs.

WILEY-*SmartMat*
Open Access

Innovation Center of Suzhou Nano Science & Technology; the 111 Project

1 | INTRODUCTION

Organic light-emitting diodes (OLEDs) have garnered considerable attention because of their applications in full-color displays and lighting. During electroexcitation, singlet and triplet excitons are generated with a ratio of 1:3.[1] For high-efficiency fluorescent emitters, full utilization of singlets can be easily achieved because their direct radiation decays are spin-allowed fluorescence process (~ns). While energy pathways of triplet excitons are much more complicated and are considered key issues for the development of OLED emitters. In 2012, Adachi et al.[2] pioneered the thermally activated delayed fluorescence (TADF) mechanism in OLEDs, proposing a guideline to effectively utilize triplet excitons with pure organic materials. With a small enough energy offset (ΔE_{ST}) between the lowest excited singlet state (S_1) and lowest excited triplet state (T_1), it is feasible that triplet excitons transfer into singlets via a reverse intersystem crossing (RISC) process, and then radiate. Thus far, a large number of TADF emitters have been exploited, leading to OLEDs with record-high external quantum efficiency (EQE).[3–12] In these systems, triplet lifetime is mainly dominated by the RISC process and generally within a range from microsecond to millisecond, much longer than that of singlets. As a consequence, triplet-related annihilations, such as triplet–triplet annihilation and singlet–triplet annihilation, are the key factors to determine the electroluminescent (EL) performance of TADF.[13] They are not only the foremost reason for concentration quenching but also cause severe efficiency roll-off at high brightness.

Triplet-related annihilations stem from intermolecular electron exchange interactions and are thus sensitive to exciton distance.[14] Therefore, the current practice of doping TADF emitters in host matrixes is necessary, as it can significantly increase the interexciton distance and suppress the annihilations. Nevertheless, the doping process generally requires precise control to guarantee a stable product quality, which is unfavorable for mass production. By contrast, nondoped OLED architecture is much more attractive for a simplified device manufacturing process, structure, and thus lower production cost. However, without host matrixes to dilute the excitons, there are, so far, very few TADF materials exhibiting decent performance in nondoped OLEDs, and their performances are still much inferior to those of doped OLEDs.[15–29] The current record of nondoped OLEDs is a green TADF emitter (2Cz-DPS) with a peak EQE of 28.7% at a brightness of ~10 cd/m². However, its EQE decreases to 2.8% at a brightness of 1000 cd/m², which thus does not meet the requirements of typical commercial applications.[16]

To enhance the performance of nondoped TADF OLEDs, design strategies need to be updated. Molecules with high photoluminescence quantum yield (PLQY) and efficient RISC process are of course primary factors to be considered. Besides, avoiding triplet-related short-range interactions is also a crucial issue. Generally, this requires a molecular optimization influencing specifically the molecular packing density. Introducing physical or virtual spacers (i.e., moieties that cannot participate in triplet distributions[14] or loose packing modulated by suitable hydrogen bonds,[25] etc.) to isolate and protect the electronically active cores from Dexter-type interactions have been explored. While most recently, our group proposed another brand new concept of enabling pure TADF materials to show a "self-doping" configuration with features similar to the conventional host–guest architecture.[26] This is achieved by exploiting the fact that many TADF emitters have two stable/metastable conformations (QA: quasi-axial conformation; QE: quasi-equatorial conformation). We have found that the form with minority population can actually behave like a dopant in a matrix of the other form with majority population. That is a neat film of a TADF emitter, which can show features of a doped film as if the minority form is doped in the majority form. By carefully designing energy levels of the two forms, such that energy from the QA "matrix" can be funneled to the QE "dopant" with good TADF characteristics. One hundred percent exciton harvesting is thus theoretically feasible in such a "self-doping" neat film. Another universal approach for improving the performance of both nondoped and doped OLEDs is to enhance optical out-coupling via increasing the population of emitters with a horizontal dipole.[30–33]

In this study, we design two new TADF emitters (Trz-Py-NCS and Trz-Py-SAC), which allow us to combine all the three approaches mentioned above for the first time. The two molecules are designed to have (1) electronically protected/isolated active cores for minimizing concentration quenching, (2) dual conformations suitable for "self-doping," and (3) linear molecular shapes beneficial for higher horizontal dipole. Both emitters exhibit excellent

exciton utilization with nearly 100% PLQYs and short exciton lifetimes of around 1.2 μs in their "self-doping" neat films, corresponding to RISC rate constants (k_{RISC}) higher than $10^6 \, s^{-1}$. Moreover, owing to their linear molecular structures, neat films of both emitters exhibit extremely highly ordered horizontal orientations with order parameters S of −0.483 and −0.499, favorable for optical out-coupling. With these combined effects, the nondoped OLEDs achieve impressive performances with record-high peak EQEs and current efficiencies (CEs) of 30.8% and 110.5 cd/A for Trz-Py-NCS, and 30.3% and 99.7 cd/A for Trz-Py-SAC, respectively. More importantly, EQEs of the two devices maintain at 29.1% and 28.1% , respectively , at a brightness of 1000 cd/m². Even at a rather high brightness of 10,000 cd/m², the EQEs of the two devices are still higher than 20%. To the best of our knowledge, these high EQEs at different brightness levels have not been reported in any conventional nondoped OLEDs, proving the success of our systematic molecular design strategy.

2 | RESULTS AND DISCUSSION

2.1 | Molecular design and synthesis

First, we construct the molecular frameworks by using triazine and acridine, respectively, as the electron-withdrawing (A) and the electron-donating (D) cores. Protecting spacers are then introduced on the cores to suitably isolate them from cores in the neighboring molecules in nondoped film. For the triazine core, two phenyl spacers are used to get the D moiety (hereafter referred to as Trz). For the acridine core, either a thioxanthene or a fluorenyl spacer is used to get A moieties referred to as NCS and SAC, respectively. The D and the A cores are connected by a pyridine bridge, thus the steric hindrance between the bridge and D is evidently reduced. Instead, a more stable QA conformation is expected, endowing the emitters with dual conformations and thus can realize "self-doping" characteristics in their neat conditions. Based on the above, we developed two target compounds Trz-Py-NCS and Trz-Py-SAC. Meanwhile, we also prepared two reference compounds Trz-Ph-NCS and Trz-Ph-SAC (see their chemical structures in Supporting Information: Figure S1), by replacing the pyridine bridge with a phenyl bridge for comparison to illustrate the importance of introducing "self-doping" feature. The synthetic routes of the four compounds are depicted in Supporting Information: Scheme S1. All four compounds were fully characterized with ^1H and ^{13}C nuclear magnetic resonance spectroscopy and mass spectrometry.

2.2 | Theoretical calculations

We first perform potential energy surface scans of all the studied compounds in ground states via the density functional theory calculations by using the B3LYP/6-31g (*d*) basis set to investigate their conformational distributions. Since both the NCS and the SAC moieties are pseudoplanar segments, all the four compounds are theoretically predicted to have dual stable conformations. Like previously reported D–A-type molecules, all their QA forms with mild twists exhibit larger energy gaps with more highest occupied molecular orbital-lowest unoccupied molecular orbital (HOMO-LUMO) overlaps and thus large ΔE_{ST} values[34,35], while the highly twisted QE forms have smaller energy gaps, less HOMO-LUMO overlaps, and thus TADF characteristics. On the other hand, the potential energies and stabilities of the two forms are highly sensitive to the bridges. As shown in the Supporting Information: Figure S1, for the reference compounds Trz-Ph-NCS and Trz-Ph-SAC with phenyl rings as the bridges, the QE forms with the lowest excited states are both absolutely dominant with relative distributions of over 99%. The very low populations of QA molecules are expected to have little influence on the macroscopic properties of these two reference emitters. While for Trz-Py-NCS and Trz-Py-SAC, using pyridines as the bridges instead, the steric hindrances between the bridges and D moieties are evidently reduced, which induces a strong tendency of forming an intramolecular hydrogen bond between them. Therefore, the QA forms with high-lying excited states are estimated to be more stable than the corresponding QE forms (Figure 1). Based on the Boltzmann distribution, percentages of the QE forms are, respectively, calculated to be 39.65% for Trz-Py-NCS and 4.82% for Trz-Py-SAC. The different populations should be ascribed to the different rigidities of the pseudoplanar segments. It can be expected that in their neat amorphous films, the QE molecules will be diluted by a larger amount of QA molecules. Thus, the average effective distances between QE molecules should be more like that in a typical host–guest system rather than in a conventional nondoped system.

We then estimate the electronic distributions and energy levels of the excited states. As shown in the Supporting Information: Figures S2–S4, in all the considered conformations of the four synthesized compounds, the natural transition orbitals of the charge-transfer excited states always almost delocalize on the specific parts of the molecules (colored in red in the molecular structures in Figure 1 and Supporting Information: Figure S1), which basically overlap with the triplet distribution. These segments can be taken as the electronically active cores of the emitters. While the
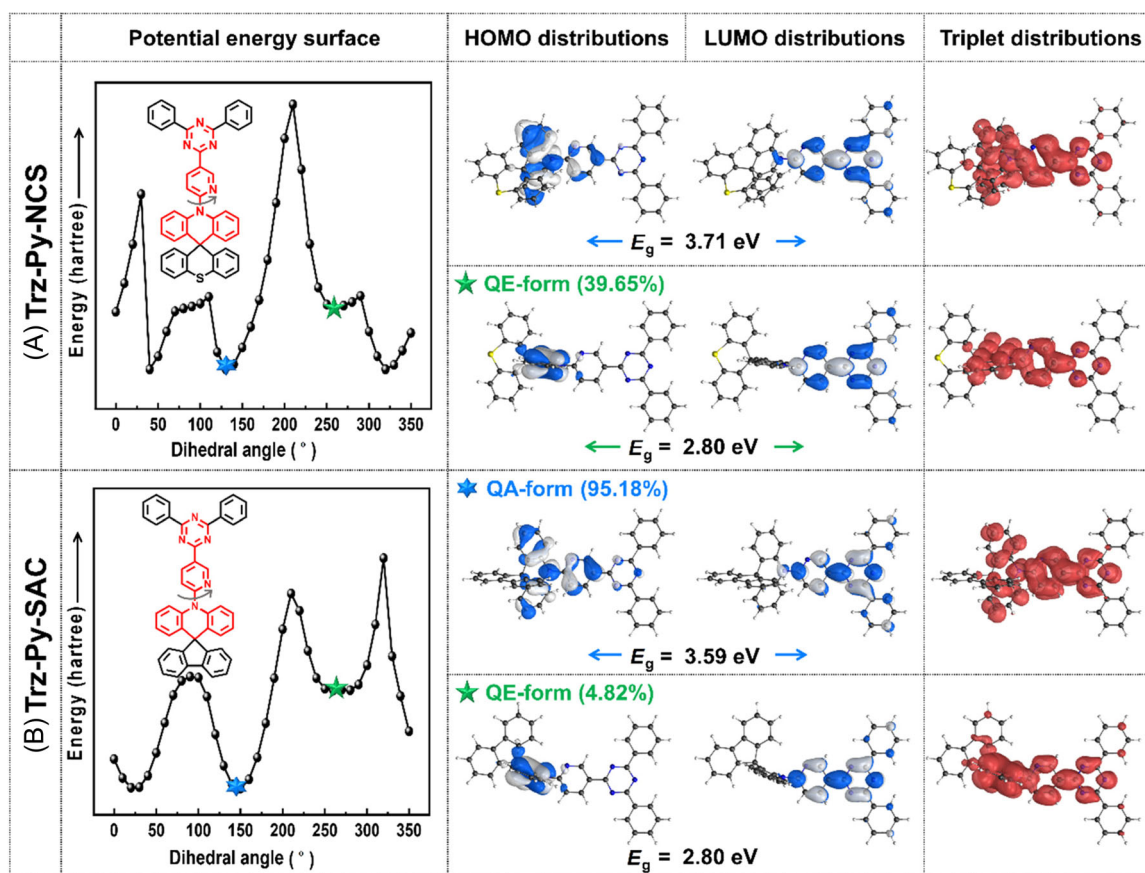
FIGURE 1 Potential energy surface scan curves, HOMO, LUMO, and triplet distributions of (A) Trz-Py-NCS and (B) Trz-Py-SAC. HOMO, highest occupied molecular orbital; LUMO, lowest unoccupied molecular orbital.

remaining segments with little triplet distributions are all peripheral, it can help in isolating the active core from interaction with neighboring active cores. These isolation effects are beneficial for suppressing the triplet-related short-range quenching, particularly when excitons are generated/passed on the few possibly aggregated QE molecules.

2.3 | Photophysics at room temperature

Photophysical properties of the studied compounds are then investigated. Figure 2 and Supporting Information: Figure S5, respectively, illustrate the absorption spectra of Trz-Py-NCS and Trz-Py-SAC diluted in dilute toluene (10^{-5} mol/L) at room temperature and those of the reference compounds (Trz-Ph-NCS and Trz-Ph-SAC) under the same condition. Due to their similar constituting components, the locally excited (LE) absorption regions are alike, while the charge-transfer (CT) bands show obviously different shapes. For Trz-Py-NCS and Trz-Py-SAC, their CT absorptions can be distinguished to be from two origins, while the reference compounds only

show weak and board bands around 395 nm from single origins. These results are well consistent with their different conformational distributions as determined by our theoretical calculations. In Supporting Information: Figure S6, CT absorption features in energy units (corresponding to ~350–450 nm) of Trz-Py-NCS and Trz-Py-SAC are further deconvoluted into two Gaussian peaks. The best-fitted peak positions for both emitters are almost the same (i.e., corresponding to wavelengths of ~372 and 416 nm). The peaks at 372 and 416 nm are ascribed to absorption of the QA and the QE conformations, respectively. The deconvolution results with molar attenuation coefficients suggest that while there is a significant amount of both QA and QE components in Trz-Py-NCS, the QE population in Trz-Py-SAC is much lower than that of the QA population.

For the PL spectra measured from their diluted toluene solution at room temperature, these emitters all show similar single broad emission peaks at ~473–507 nm. Further transient PL decay measurements (shown in Supporting Information: Figure S7) on these emission maxima show that they all exhibit similar two-component decays under nitrogen atmosphere
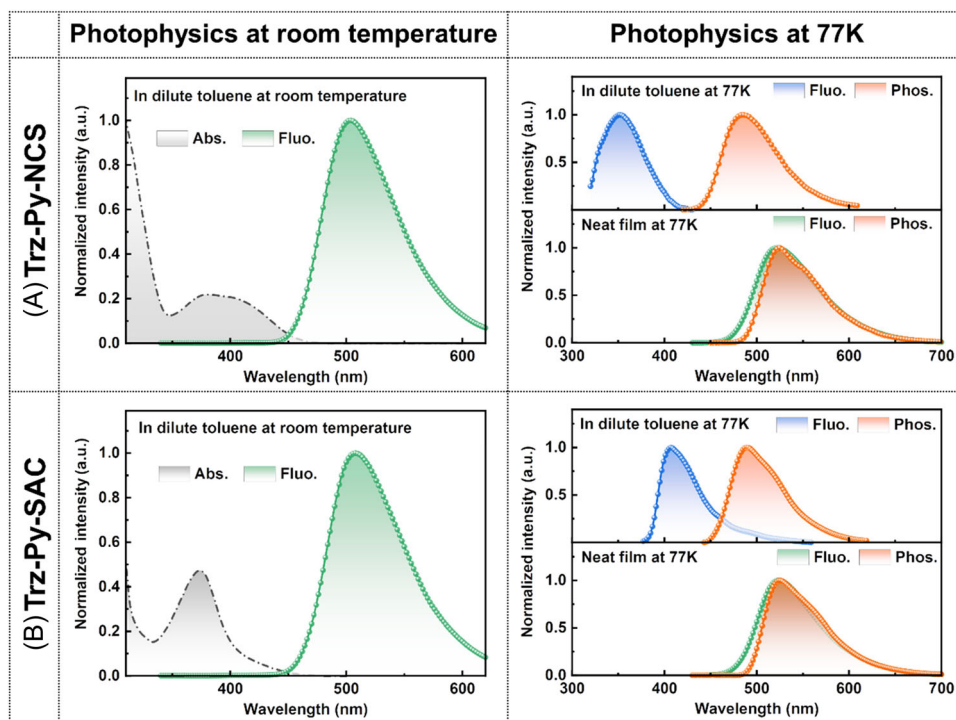
FIGURE 2 Ultraviolet–visible absorption (dashed line) and fluorescence spectra (solid line) in dilute toluene at room temperature; fluorescence and phosphorescence spectra in dilute toluene (top) and nondoped films (bottom) at 77 K of (A)Trz-Py-NCS and (B) Trz-Py-SAC.

respectively in the ranges of nanosecond and microsecond. However, after oxygen bubbling, the micro second-scale signals are significantly quenched, indicating their TADF features. Moreover, these emissions all show typical redshifts with increasing environmental polarities due to the solvatochromic effect (Supporting Information: Figure S8). These results are in good agreement with the expected properties of their QE conformations, while the signals of QA conformations can barely be detected because of the molecular relaxation (Supporting Information: Figure S9) and exciton energy transfer process.[36]

2.4 | Photophysics at 77 K

We further measured fluorescence and phosphorescence spectra of Trz-Py-NCS and Trz-Py-SAC diluted in toluene at 77 K to fix molecular conformations and block the energy transfer between different conformations such that we have a chance to obtain the energy level information of high-lying forms.[37,38] As shown in Figure 2, both fluorescence spectra were observed with peaks around 400 nm, significantly blue-shifted compared to those at room temperature, which should be ascribed to their QA forms. By using the corresponding onsets, the S_1 and T_1 levels of QA forms were calculated to be 3.52 and

2.80 eV for Trz-Py-NCS and 3.23 and 2.74 eV for Trz-Py-SAC, thereby ΔE_{ST} values were determined to be 720 and 490 meV, too large to activate efficient RISC processes. To determine the S_1 and T_1 energy levels of the QE forms, we also measured the fluorescence and phosphorescence spectra of all the four compounds from their neat films at 77 K in which the energy transfer from QA to QE forms should be sufficient (Figure 2). As summarized in Supporting Information: Table S1, energy levels of all the QE forms are lower than the corresponding results of the QA forms, ensuring that the QA molecules can act as host matrixes for the QE ones. Furthermore, ΔE_{ST} values of the QE forms of the four compounds are estimated to be 58–87 meV. Such low ΔE_{ST} values would give rise to their efficient TADF features.

2.5 | Characterizations based on single crystals

To build convinced connections between their macroscopic properties and microscopic geometries, we tried to obtain different single crystals of Trz-Py-NCS and Trz-Py-SAC by using the liquid-phase diffusion method under various conditions. For Trz-Py-SAC, we succeeded in getting two kinds of single crystals, which were further analyzed to contain two different conformations.

Figure 3 shows the two different geometries obtained from X-ray powder diffraction analyses of the two Trz-Py-SAC single crystals. The dihedral angles are, respectively, 21.79° and 78.53°, which can be identified as QA and QE forms in theoretical simulations. While for Trz-Py-NCS, we can only obtain one kind of single crystal, which is corresponding to the QE form. The slight geometry differences between the estimation and that in the crystal are reasonable for their different environments.

Supporting Information: Figures S10–S12 show the packing patterns of Trz-Py-NCS and Trz-Py-SAC obtained from their single crystals. In all these packings, obvious steric hindrances provided by NCS and SAC moieties obviously suppress close π–π stacking of D moieties and thus help to isolate excitons from each other. While on the A-side, the peripheral phenyl groups attached to the triazine cores with very good planarity. Thus, they can only well protect environmental interactions from the in-plane direction, while from the out-of-plane direction, obvious triazine stacking can be noticed, which may also lead to a risk of triplet-related quenching process. Thus, doping the molecules in a host matrix should still be needed for better exciton utilization.

We further compared the photophysical behaviors of Trz-Py-SAC and Trz-Py-NCS in nondoped films and crystals to confirm the influence of different conformations. As shown in the Supporting Information: Figure S14, for the neat films, when detecting at the QA emission maxima, the relative intensities in the high-energy excited regions (i.e., corresponding to the LE states) are weaker than those detected at the QE emission maxima because of the absence of absorption of QE forms. Figure 3A displays the excitation-dependent spectra of Trz-Py-SAC neat film and its two kinds of crystals at their emission maxima. The strong CT absorption band at 370 nm determined from the QA crystal well remains in the nondoped film. While the observed CT intensity reflected at 430 nm in the QE crystal becomes very weak in the nondoped film. These results further confirm the low population of QE molecules in Trz-Py-SAC nondoped film. Interestingly, the PL spectrum of the nondoped film is much more like that of the QE crystal rather than the QA crystal, indicating a sufficient energy transfer occurrence from the high population QA to the low population QE forms in the nondoped film (Figure 3B). Meanwhile, for Trz-Py-NCS, although the QA crystal cannot be grown, the other comparisons between the nondoped films and the obtained QE crystal are very similar to the corresponding results of Trz-Py-SAC (Supporting Information: Figure S13), indicating their
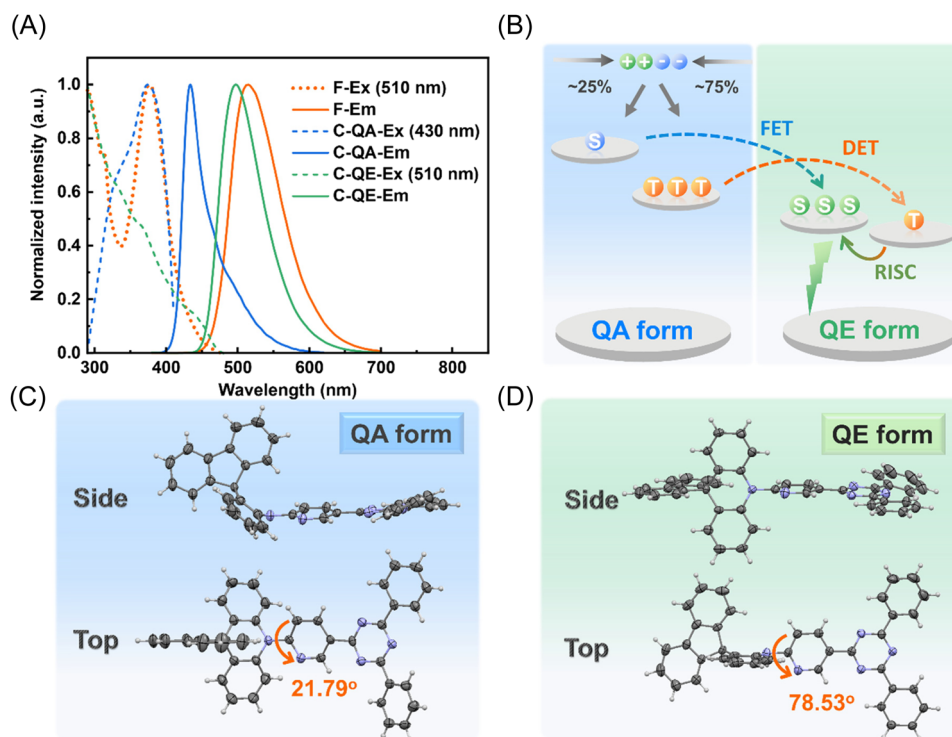
FIGURE 3 (A) Fluorescence spectra (solid line) of nondoped film (orange), QA-form crystal (blue), QE-form crystal (green), and the corresponding excitation-dependent spectra (dashed line) of Trz-Py-SAC. (B) Model of energy transfer between QA and QE forms. ORTEP drawings of (C) QA- and (D) QE-form crystals. ORTEP, Oak Ridge Thermal Ellipsoid Plot Program; QA, quasi-axial conformation; QE, quasi-equatorial conformation.

similar conformational distributions in nondoped conditions. The high-lying QA conformations with higher populations would play as host matrices to dilute the QE molecules, and avoid the concentration quenching as second insurance on top of steric hindrance.

2.6 | PLQY and kinetic analyses

To further investigate the exciton utilization of these compounds in different dilutions, PLQYs of the studied compounds were evaluated by diluting them in host matrixes with various concentrations (Trz-Py-NCS and Trz-Py-SAC were doped in 1,3-di(9H-carbazol-9-yl) benzene [mCP], while Trz-Ph-NCS and Trz-Ph-SAC were doped in bis[2-(diphenylphosphino)phenyl] ether oxide [DPEPO]). As shown in the Supporting Information: Figure S15, for the reference compounds Trz-Ph-NCS and Trz-Ph-SAC, with increasing doping concentrations from 20 to 100 wt% (i.e., nondoped), the PLQYs all maintained higher than 75%, revealing their well-suppressed concentration quenching. While on the other hand, there are still mild but clear declines, indicating the issue of concentration quenching is still remaining. While for Trz-Py-NCS and Trz-Py-SAC, their PLQYs show little changes with concentrations varied over the same range. Impressively, in nondoped films, both Trz-Py-NCS and Trz-Py-SAC realize PLQYs of 100%. Apparently, the fact that the emissive QE molecules are actually diluted in the host QA molecules contributes to the excellent exciton utilization.

We then carried out the transient decay measurement to analyze the detailed kinetic process. As shown in Supporting Information: Figure S16, temperature-dependent PL decay curves of their nondoped films show obvious TADF features. Particularly, at 300 K the delayed lifetimes were determined to be as short as 1.2 and 1.3 μs for Trz-Py-NCS and Trz-Py-SAC, respectively.

The corresponding kinetic parameters were further calculated and summarized in Supporting Information: Table S2. Trz-Py-NCS and Trz-Py-SAC nondoped films are both estimated to have high k_{RISC} values $>10^6 \, s^{-1}$. Such a rapid RISC process would be beneficial for suppressing triplet-related quenching at high exciton densities and thus reduce efficiency roll-off at high brightness.

We also compared transient decays of these compounds in various doping concentrations to further confirm the origin of their different concentration sensitivities. As shown in the Supporting Information: Figure S17, with the increase in concentration, the TADF components show similar contributions for Trz-Py-NCS and Trz-Py-SAC, while for the two reference compounds, we observed no obvious decrease in their delayed components' contributions at high concentrations due to triplet-related concentration quenching. These differences further confirmed that the nonradiative deactivation processes caused by concentration quenching have been ideally addressed by combining the steric hindrance molecular design and "self-doping" strategy.

2.7 | Out-coupling factors

Generally, emitters with linear molecular structures, such as Trz-Py-NCS and Trz-Py-SAC, could possibly realize highly ordered horizontal orientations and thus significantly enhance the optical out-coupling in OLEDs. Thus, we further evaluated the orientation of Trz-Py-NCS- and Trz-Py-SAC-based nondoped films via the variable angle spectroscopic ellipsometry measurement. As depicted in Figure 4, there are remarkable differences between the optical constant curves of ordinary and extraordinary, revealing the nonrandom orientations of both compounds. Further quantitative analysis confirms that the two emitters possess highly ordered horizontal
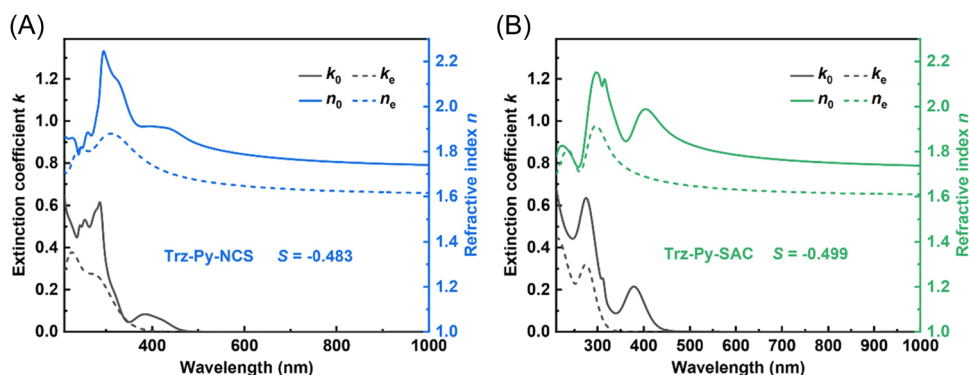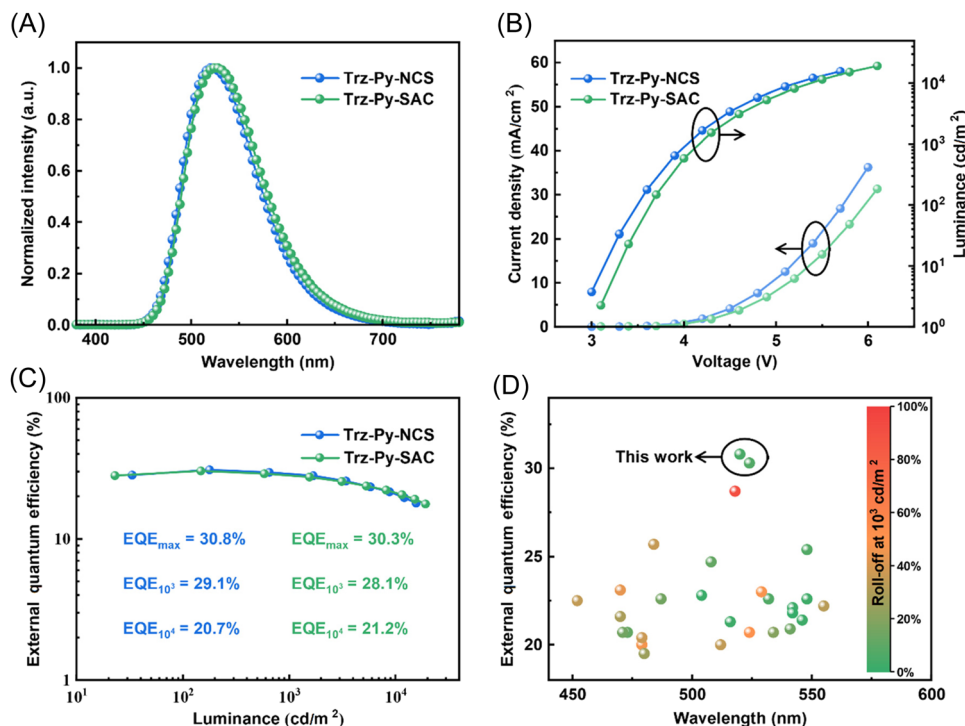

FIGURE 4 Optical anisotropy results of (A) Trz-Py-NCS and (B) Trz-Py-SAC in extinction coefficient k and refractive index n with the ordinary (solid) and extraordinary optical constants (dashed) curves.

FIGURE 5 EL performance of nondoped OLEDs based on Trz-Py-NCS and Trz-Py-SAC. (A) EL spectra at 1000 cd/m^2; (B) voltage–luminance–current density characteristics; (C) external quantum efficiency–luminance curves; (D) summary of nondoped OLEDs with EQE exceeding 20% (color map insert is to compare the efficiency roll-off at 1000 cd/m^2). EL, electroluminescent; EQE, external quantum efficiency; OLED, organic light-emitting diode.

orientations with order parameters S of −0.483 and −0.499.[39] To the best of our knowledge, these values are among the highest of the reported TADF emitters. Such high horizontal orientations would further benefit them to realize superior EQEs in devices.[32]

2.8 | EL performance

To compare the EL performance of these emitters in different conditions, we fabricated OLED devices with the following architecture (see details in Supporting Information: Figure S18): indium tin oxide/4,4′-(cyclo hexane-1,1-diyl)bis(*N*,*N*-di-*p*-tolylaniline) (ITO/TAPC) (40 nm)/tris(4-(9*H*-carbazol-9-yl)phenyl)amine (TCTA) (10 nm)/mCP (10 nm)/emitting layer (20 nm)/3,3′-(5′-(3-(pyridin-3-yl)phenyl)-[1,1′:3′,1″-terphenyl]-3,3″-diyl)dipy ridine (TmPyPB) (45 nm)/LiF (1 nm)/Al in which ITO and LiF/Al are used as the anode and the cathode, respectively. Both TAPC and TCTA served as hole-injection layer; mCP and TmPyPB are sequentially used as the exciton-blocking layer and electron-transporting layer; mCP is also chosen as the host material for Trz-Py-NCS and Trz-Py-SAC, while DPEPO is used as the host for Trz-Ph-NCS and Trz-Ph-SAC due to their different T$_1$ energy levels.

The nondoped OLEDs based on the reference compounds Trz-Ph-NCS and Trz-Ph-SAC, respectively, realized maximum EQEs of 19.1% and 17.4%, respectively, which are quite reasonable among all TADF-based nondoped OLEDs, indicating the effectiveness of using the steric hindrance groups for protecting the electronically active cores. However, their efficiency roll-offs are less satisfactory at high brightness, indicating using only the "isolating emitting cores" strategy is not efficacious enough to sufficiently suppress triplet-related quenching in these nondoped films. On the other hand, these device series still exhibit typical optimizing curves in which the efficiencies increased to the maxima with doping ratios increased to 20–30 wt% and then dropped afterward, indicating that a host matrix is still required for further diluting the emitter for suppressing concentration quenching. More importantly, these performances are much inferior to the overall behaviors of Trz-Py-NCS- and Trz-Py-SAC-based devices (see Supporting Information: Figure S19). With a doping concentration of 5 wt%, high EQEs of ∼22.9% and 24.3% were obtained, respectively, for the Trz-Py-NCS and Trz-Py-SAC devices. By further increasing doping ratios, both device series showed overall upward trends in their efficiencies, agreeing well with their PLQY results (Supporting Information: Tables S3 and S4). Their results reveal the

TABLE 1 EL performance of nondoped OLEDs for Trz-Py-NCS and Trz-Py-SAC.

TADF emitter	V_{on}[a] (V)	λ_{EL} (nm)	EQE/CE/PE[b] [%/(cd/A)/(lm/W)]			Roll-off[c] (%)
			@maximum	@1000 cd/m^2	@10,000 cd/m^2	
Trz-Py-NCS	3.1	520	30.8/100.5/95.0	29.1/94.0/73.8	20.7/70.1/40.4	5.5
Trz-Py-SAC	3.3	524	30.3/99.7/85.3	28.1/92.6/69.2	21.2/67.8/40.8	7.3

Abbreviations: CE, current efficiency; EL, electroluminescent; EQE, external quantum efficiency; OLED, organic light-emitting diode; PE, power efficiency; TADF, thermally activated delayed fluorescence.

[a]Turn-on voltage measured at 10 cd/m^2.

[b]External quantum efficiency, current efficiency, and power efficiency.

[c]External quantum efficiency roll-off from maximum value to that at 1000 cd/m^2.

importance of owning considerable populations of the QE molecules in exciton utilization.[40] Moreover, better carrier balances with increasing doping concentrations should also contribute to the increased efficiencies and reduced roll-offs (see Supporting Information: Figure S21 for details). Specifically, Figure 5 and Supporting Information: Figure S20 illustrate the EL performance of the nondoped OLEDs based on these emitters, and detailed information is included in Table 1 and Supporting Information: Table S5. Both nondoped devices of Trz-Py-NCS and Trz-Py-SAC exhibit lower turn-on voltages than their corresponding doped devices. Intriguingly, the nondoped OLEDs based on Trz-Py-NCS and Trz-Py-SAC achieve record-high peak EQEs and CEs of 30.8% and 110.5 cd/m for Trz-Py-NCS and 30.3% and 99.7 cd/m for Trz-Py-SAC. Moreover, EQEs of the two devices are both higher than 28% and 20% even at a high brightness of 1000 and 10,000 cd/m^2, respectively. To the best of our knowledge, these high EQEs over such a wide range of brightness levels have not been reported in any conventional nondoped OLEDs (Supporting Information: Table S6), indicating the effectiveness of the present synergetic molecular design strategy.

3 | CONCLUSION

Two new TADF emitters are designed by incorporating three design approaches for enhancing neat electroluminescence performance. The strategic designs involve (1) employing bulky peripheral side groups to protect/isolate excitation core from interacting with each other; (2) using a D–A linking bridge, which enables dual conformations leading to a low energy TADF conformer "doped" in a high-energy fluorescent conformer; and (3) linear molecular shape for enhancing horizontal dipole and optical out-coupling. With the first two approaches, the two new TADF emitters achieve nearly 100% exciton harvesting even in their nondoped films. Combining with the good optical out-coupling, OLEDs using the two new emitters deliver record-high maximum EQEs of over 30%

for the first time in nondoped OLEDs. The two devices also show minimal efficiency roll-off at high brightness, which is unprecedented among nondoped OLEDs.

CONFLICTS OF INTEREST
The authors declare no conflicts of interest.

DATA AVAILABILITY STATEMENT
The data that support the findings of this study are available in the supplementary material of this article.

ORCID
Xiao-Chun Fan https://orcid.org/0000-0002-4628-8228
Kai Wang https://orcid.org/0000-0002-9860-2282
Yi-Zhong Shi https://orcid.org/0000-0002-8397-9618
Xiao-Hong Zhang https://orcid.org/0000-0002-6732-2499

REFERENCES
1. Baldo MA, O'Brien DF, Thompson ME, Forrest SR. Excitonic singlet-triplet ratio in a semiconducting organic thin film. *Phys Rev B*. 1999;60(20):14422-14428.
2. Uoyama H, Goushi K, Shizu K, Nomura H, Adachi C. Highly efficient organic light-emitting diodes from delayed fluorescence. *Nature*. 2012;492(7428):234-238.
3. Wu TL, Huang MJ, Lin CC, et al. Diboron compound-based organic light-emitting diodes with high efficiency and reduced efficiency roll-off. *Nat Photon*. 2018;12(4):235-241.
4. Karthik D, Jung YH, Lee H, et al. Acceptor–donor–acceptor-type orange-red thermally activated delayed fluorescence materials realizing external quantum efficiency over 30% with low efficiency roll-off. *Adv Mater*. 2021;33(18):2007724.

5. Chen YK, Jayakumar J, Hsieh CM, et al. Triarylamine–pyridine–carbonitriles for organic light-emitting devices with EQE nearly 40%. *Adv Mater.* 2021;33(35):2008032.

6. Chen Y, Zhang D, Zhang Y, et al. Approaching nearly 40% external quantum efficiency in organic light emitting diodes utilizing a green thermally activated delayed fluorescence emitter with an extended linear donor-acceptor-donor structure. *Adv Mater.* 2021;33(44):2103293.

7. Zhang Y, Wei J, Zhang D, et al. Sterically wrapped multiple resonance fluorophors for suppression of concentration quenching and spectrum broadening. *Angew Chem Int Ed.* 2022;61(2):202113206.

8. Zeng X, Huang YH, Gong S, et al. An unsymmetrical thermally activated delayed fluorescence emitter enables orange-red electroluminescence with 31.7% external quantum efficiency. *Mater Horiz.* 2021;8(8):2286-2292.

9. Kondo Y, Yoshiura K, Kitera S, et al. Narrowband deep-blue organic light-emitting diode featuring an organoboron-based emitter. *Nat Photon.* 2019;13(10):678-683.

10. Cai Z, Wu X, Liu H, et al. Realizing record-high electroluminescence efficiency of 31.5% for red thermally activated delayed fluorescence molecules. *Angew Chem Int Ed.* 2021;60(44):23635-23640.

11. Wei J, Zhang C, Zhang D, et al. Indolo[3,2,1-*jk*]carbazole embedded multiple-resonance fluorophors for narrowband deep-blue electroluminescence with EQE approximately 34.7% and CIEy approximately 0.085. *Angew Chem Int Ed.* 2021; 60(22):12269-12273.

12. Li W, Li M, Li W, et al. Spiral donor design strategy for blue thermally activated delayed fluorescence emitters. *ACS Appl Mater Interfaces.* 2021;13(4):5302-5311.

13. Hasan M, Shukla A, Ahmad V, et al. Exciton–exciton annihilation in thermally activated delayed fluorescence emitter. *Adv Funct Mater.* 2020;30(30):2000580.

14. Lee J, Aizawa N, Numata M, Adachi C, Yasuda T. Versatile molecular functionalization for inhibiting concentration quenching of thermally activated delayed fluorescence. *Adv Mater.* 2017;29(4):1604856.

15. Kim JU, Park IS, Chan CY, et al. Nanosecond-time-scale delayed fluorescence molecule for deep-blue OLEDs with small efficiency rolloff. *Nat Commun.* 2020;11(1):1765.

16. Yang Z, Mao Z, Xu C, et al. A sterically hindered asymmetric D–A–D′ thermally activated delayed fluorescence emitter for highly efficient non-doped organic light-emitting diodes. *Chem Sci.* 2019;10(35):8129-8134.

17. Matsuo K, Yasuda T. Blue thermally activated delayed fluorescence emitters incorporating acridan analogues with heavy group 14 elements for high-efficiency doped and non-doped OLEDs. *Chem Sci.* 2019;10(46):10687-10697.

18. Huang J, Nie H, Zeng J, et al. Highly efficient nondoped OLEDs with negligible efficiency roll-off fabricated from aggregation-induced delayed fluorescence luminogens. *Angew Chem Int Ed.* 2017;56(42):12971-12976.

19. Huang Z, Bin Z, Su R, Yang F, Lan J, You J. Molecular design of non-doped OLEDs based on a twisted heptagonal acceptor: a delicate balance between rigidity and rotatability. *Angew Chem Int Ed.* 2020;59(25):9992-9996.

20. Park IS, Min H, Kim JU, Yasuda T. Deep-blue OLEDs based on organoboron–phenazasiline-hybrid delayed fluorescence emitters

21. Zhang Q, Tsang D, Kuwabara H, et al. Nearly 100% internal quantum efficiency in undoped electroluminescent devices employing pure organic emitters. *Adv Mater.* 2015;27(12): 2096-2100.

22. Lin TA, Chatterjee T, Tsai WL, et al. Sky-blue organic light emitting diode with 37% external quantum efficiency using thermally activated delayed fluorescence from spiroacridine–triazine hybrid. *Adv Mater.* 2016;28(32):6976-6983.

23. Wang YF, Li M, Teng JM, Zhou HY, Chen CF. High-performance solution-processed nondoped circularly polarized OLEDs with chiral triptycene scaffold-based TADF emitters realizing over 20% external quantum efficiency. *Adv Funct Mater.* 2021;31(49):2106418.

24. Gan L, Xu Z, Wang Z, et al. Utilizing a spiro TADF moiety as a functional electron donor in TADF molecular design toward efficient "multichannel" reverse intersystem crossing. *Adv Funct Mater.* 2019;29(20):1808088.

25. Shi Y, Wang K, Tsuchiya Y, et al. Hydrogen bond-modulated molecular packing and its applications in high-performance non-doped organic electroluminescence. *Mater Horiz.* 2020; 7(10):2734-2740.

26. Shi YZ, Wang K, Zhang SL, et al. Characterizing the conformational distribution in an amorphous film of an organic emitter and its application in a "self-doping" organic light-emitting diode. *Angew Chem Int Ed.* 2021;60(49):25878-25883.

27. Rizzo F, Cucinotta F. Recent developments in AIEgens for non-doped and TADF OLEDs. *Isr J Chem.* 2018;58(8):874-888.

28. Godumala M, Choi S, Cho MJ, Choi DH. Recent breakthroughs in thermally activated delayed fluorescence organic light emitting diodes containing non-doped emitting layers. *J Mater Chem C.* 2019;7(8):2172-2198.

29. Hong X, Zhang D, Yin C, et al. TADF molecules with π-extended acceptors for simplified high-efficiency blue and white organic light-emitting diodes. *Chem.* 2022. doi:10.1016/j. chempr.2022.02.017

30. Sun Y, Forrest SR. Enhanced light out-coupling of organic light-emitting devices using embedded low-index grids. *Nat Photon.* 2008;2(8):483-487.

31. Reineke S, Lindner F, Schwartz G, et al. White organic light-emitting diodes with fluorescent tube efficiency. *Nature.* 2009; 459(7244):234-238.

32. Watanabe Y, Sasabe H, Kido J. Review of molecular engineering for horizontal molecular orientation in organic light-emitting devices. *Bull Chem Soc Jpn.* 2019;92(3):716-728.

33. Lee YT, Tseng PC, Komino T, et al. Simple molecular-engineering approach for enhancing orientation and out-coupling efficiency of thermally activated delayed fluorescent emitters without red-shifting emission. *ACS Appl Mater Interfaces.* 2018;10(50):43842-43849.

34. Tanaka H, Shizu K, Nakanotani H, Adachi C. Dual intramolecular charge-transfer fluorescence derived from a phenothiazine-triphenyltriazine derivative. *J Phys Chem C.* 2014;118(29):15985-15994.

35. Ward JS, Nobuyasu RS, Fox MA, et al. Bond rotations and heteroatom effects in donor–acceptor–donor molecules: implications for thermally activated delayed fluorescence and room temperature phosphorescence. *J Org Chem.* 2018;83(23):14431-14442.

36. Li F, Li M, Fan J, Song Y, Wang CK, Lin L. Theoretical study on thermally activated delayed fluorescence emitters in white organic light-emitting diodes: emission mechanism and molecular design. *J Phys Chem A*. 2020;124(37): 7526-7537.

37. Wang K, Zheng CJ, Liu W, et al. Avoiding energy loss on TADF emitters: controlling the dual conformations of D–A structure molecules based on the pseudoplanar segments. *Adv Mater*. 2017;29(47):1701476.

38. Wang K, Shi YZ, Zheng CJ, et al. Control of dual conformations: developing thermally activated delayed fluorescence emitters for highly efficient single-emitter white organic light-emitting diodes. *ACS Appl Mater Interfaces*. 2018;10(37):31515-31525.

39. Kaji H, Suzuki H, Fukushima T, et al. Purely organic electroluminescent material realizing 100% conversion from electricity to light. *Nat Commun*. 2015;6:8476.

40. Moon YK, Jang HJ, Hwang S, et al. Modeling electron-transfer degradation of organic light-emitting devices. *Adv Mater*. 2021;33(12):2003832.

SUPPORTING INFORMATION

Additional supporting information can be found online in the Supporting Information section at the end of this article.

How to cite this article: Fan X-C, Wang K, Shi Y-Z, et al. Thermally activated delayed fluorescence materials for nondoped organic light-emitting diodes with nearly 100% exciton harvest. *SmartMat*. 2023;4:e1122. doi:10.1002/smm2.1122